Int J Fract (2010) 165:93–103
DOI 10.1007/s10704-010-9508-3

ORIGINAL PAPER

Damage and plasticity in adhesive layer: an experimental study

Anders Biel · Ulf Stigh

Received: 10 January 2010 / Accepted: 18 May 2010 / Published online: 9 June 2010

Abstract An experimental method is developed to identify a suitable model of in-elastic behaviour of an adhesive layer. Two prototype models are considered: an elastic-plastic model where the in-elasticity is considered due to permanent straining of the adhesive and an elastic-damage model where the in-elasticity is due to a reduction in elastic stiffness. Simulations show that the evaluated property is sensitive to the choice of model. In the experimental study of an engineering epoxy adhesive, the elastic-damage model fits the experiments. The study also reveals that plasticity and damage accumulated at the crack tip influences the evaluated fracture properties.

Keywords Adhesive · Epoxy · Elastic-damage · Elastic-plastic · DCB-specimen · Peel · R-curve

1 Introduction

Cohesive laws are used in simulations to predict the behaviour of adhesively joined structures, cf. e.g. Li et al. (2006). In the automotive and aeronautic industries, these models are currently considered in the development of new design methods. Commercial FE-software now includes cohesive elements and models (e.g. Abaqus and LS-Dyna). Three levels of complexity can be identified to model an adhesive joint. In Salomonsson and Andersson (2008), the adhesive is considered as a composite material. By use of cohesive elements located between all finite elements in the mesh, cracks are allowed to initiate and grow within the adhesive. Tvergaard and Hutchinson (1996) use one cohesive zone embedded in an elastic plastic model of the adhesive layer. The adhesive is confined between stiff adherends loaded by an external K-field, thus modelling small scale yielding. Both of these models are too detailed to be used in simulations of complex built-up structures. To this end, the *adhesive layer model* has proven successful in representing the major properties of the adhesive. In this model, the adhesive layer with thickness t is considered loaded in an arbitrary combination of peel (w, σ) and shear (v, τ), cf. Fig. 1. In 3D, the shear component is split in two orthogonal components. The relations between the tractions, σ, τ, and the deformations, w, v, are given by a cohesive law. Thus, the cohesive law reflects the homogenized properties of the adhesive layer. In this way, the cohesive law can be regarded as a constitutive property of the adhesive layer, cf. Stigh et al. (2009). These properties are known to depend on the thickness of the layer, cf. Kafkalidis et al. (2000) and Carlberger and Stigh (2009).

The properties of the cohesive law reflect the mechanisms of deformation and fracture. With monotonically increasing deformation of the adhesive layer, the nature of these mechanisms is usually of minor importance in a structural analysis. However, with varying loading, as expected in most applications, the nature of

A. Biel (✉) · U. Stigh
University of Skövde, Skövde, Sweden
e-mail: Anders.Biel@his.se
URL: http://www.his.se\MechMat

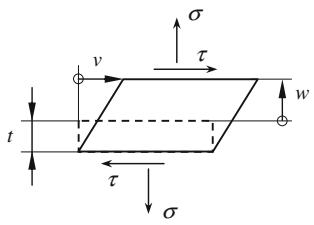

Fig. 1 Deformation modes of the adhesive layer with thickness t: peel, w, and shear, v. Conjugated stress components σ and τ

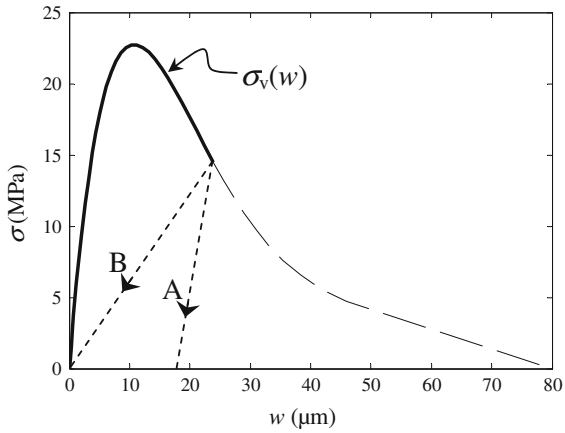

Fig. 2 Cohesive law for the epoxy adhesive DOW-Betamate XW 1044-3. **a** *elastic-damage* **b** *elastic-plastic*

the mechanisms is important. Three basic models are usually considered: elasticity, plasticity and damage, cf. e.g. Alfredsson and Stigh (2004). Figure 2 illustrates these mechanisms for a cohesive law loaded in peel. In monotonically increasing elongation, w, of the adhesive layer the traction-separation relation $\sigma_v(w)$ results. The area under this curve is identified as the fracture energy of the adhesive layer.

Plasticity is manifested by a remnant deformation upon unloading from an inelastic state, cf. path A in Fig. 2. Plasticity can be more or less time dependent. It may also be associated with elastic after effects whereby the remnant plastic deformation decreases with time after unloading. Damage appears as decreasing elastic stiffness attributed to nucleation and growth of micro cavities, cf. path B in Fig. 2. These two models, plasticity and damage reflect deformation mechanisms on a smaller length scale. For crystalline solids, plasticity is due to the nucleation and motion of dislocations. Time dependent plasticity may also be due to diffusion. Nucleation and growth of cavities result in damage. Plasticity and damage can be used as

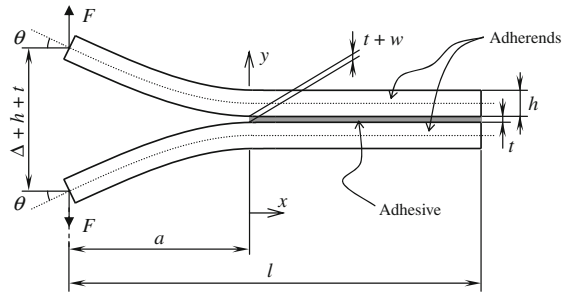

Fig. 3 DCB-specimen, the out-of-plane width of the specimen is b

basic mechanisms to model the inelastic properties of an adhesive layer. Efforts to discriminate between plasticity and damage in adhesive layers are relatively sparse. Salomonsson (2008) use a mesomechanical model of an engineering epoxy to study effects of the mode mix on cohesive laws, i.e. combinations of w and v. He concludes that virtually no plasticity occurs in peel loading. In shear loading, plasticity is responsible for the larger fracture energy of the adhesive layer. The present authors are not aware of any experimental study to identify plasticity and damage in adhesive layers.

Experimental methods to measure cohesive laws in pure peel loading are developed in Olsson and Stigh (1989); Suo et al. (1992); Sørensen and Jacobsen (1998) and Stigh and Andersson (2000). In shear loading, methods are developed in Alfredsson (2004), and Leffler et al. (2007). The double cantilever beam (DCB) specimen is used to measure cohesive laws in peel, cf. e.g. Andersson and Stigh (2004) and Fig. 3.

The method to measure cohesive laws is based on the path-independence of the J-integral,

$$J \equiv \int_S \left(W n_x - \sigma_{ik} u_{i,x} n_k \right) \mathrm{d}S \tag{1}$$

where W, σ, $\mathbf{u}$ and $\mathbf{n}$ are the strain energy density, the stress tensor, the displacement vector and the unit outward normal to the counter-clockwise path S encircling the start of the adhesive layer; repeated indexes indicate summation and the coordinate system is given in Fig. 3. If W is not explicitly dependent of x, J is independent of the path S. Moreover, if W cannot be defined, i.e. if the material is inelastic, J can still be path independent. This is the case if a pseudo potential can be assigned to the stress-strain relation of the material, cf. e.g. Nilsson (2001). Taking an integration path at the start of the adhesive layer gives,

$$J = \int_t W \mathrm{d}y \tag{2}$$

Utilizing an alternative integration path at the exterior boundary gives,

$$J = \frac{2F\theta}{b} \tag{3}$$

where F is the applied force, θ is the rotation and b the width of the specimen. Thus, by measuring F and θ continuously during an experiment and equating Eq.'s 2 and 3, a primitive function to the strain energy density is determined. The cohesive law is then determined by differentiation,

$$\sigma(w) = \frac{\mathrm{d}J}{\mathrm{d}w} \tag{4}$$

where w is the deformation of the adhesive at the start of the adhesive layer, cf. Fig. 3. The differentiation of the experimental result is made by first adapting a Prony series to the experimental J vs. w data, cf. Fernberg and Berglund (2001). Cohesive laws have been derived in several studies of adhesive behaviour. Andersson and Biel (2006) show that the measured cohesive law is virtually independent of the thickness of the adherends; Leffler et al. (2007) and Zhu et al. (2009) show rate dependence in shear loading; Carlberger et al. (2009) measure effects of temperature and strain rate; Carlberger and Stigh (2009) studies effects of the thickness of the adhesive layer. An alternative method where the specimen is loaded by bending moments instead of transversal forces is used by Sørensen (2002).

These methods are only valid for adhesive layers with homogenous properties along the layer, i.e. with W independent of any explicit dependence on x. The influence of a variation of constitutive properties along the layer will depend on the size of the stressed zone preceding the crack tip, i.e. the material used for determining the energy release rate. The size of this zone is dependent of the bending stiffness of the adherends and the constitutive relation of the adhesive layer. Effects of varying properties along the adhesive layer are studied by Biel (2005). He identifies several possible sources for varying properties:

- voids due to trapped air during the hardening process
- varying adhesive layer thickness
- residual stresses
- moisture
- varying strain rate along the adhesive layer

Voids can often be identified after the experiment and the experiment can be rejected. A variation of the layer thickness can be identified before the experiment. Residual stresses are more difficult to analyse. In-plane residual stresses (σ_{xx}) are expected in thermosetting adhesives due to differences in thermal expansion between the adhesive and the adherends. Effects are studied based on linear elasticity in e.g. Fleck et al. (1991) and Guo et al. (2006). The applicability of these results for tough engineering epoxies remains to be studied. Transversal residual stresses (σ_{yy}) can also occur, though the resultants of these stresses must be zero by equilibrium. Without too long time between manufacturing of specimens and testing, moisture should not be a problem. Carlberger et al. (2009) examines the influence of strain rate on the properties of the present adhesive. They show only minor influences of the strain rate on the cohesive laws. It may also be noted that pre-loading appears frequently in order to achieve a sharp crack tip. For instance, a wedge or fatigue loading can be used to propagate the crack tip in order to avoid the man-made crack tip region in a specimen.

The main goal of the present paper is to identify experimentally if plasticity or damage is best suited to represent the in-elastic properties of an adhesive loaded in peel. We will also study effects of the pre-loading frequently performed in fracture mechanics testing. The adhesive is DOW-Betamate XW 1044-3 with layer thickness $t = 0.2$ mm. This is an adhesive used by the automotive industry. It consists of a blend of epoxy and a thermoplastic with needled shaped mineral particles, cf. Salomonsson and Andersson (2008). The adhesive has been evaluated thoroughly in earlier studies, cf. e.g. Andersson and Biel (2006) and Leffler et al. (2007).

The procedure to identify plasticity and damage is as follows. A DCB-specimen is first loaded to a predefined inelastic state and then unloaded. During this stage, a zone of in-elastically deformed adhesive is created at the start of the layer. In step 2, the specimen is reloaded and evaluated as if the specimen is in its *virgin state*. That is, we pretend not to know about the first loading step. As shown in the next section, simulations show that the present evaluation method is sensitive to the origin of the inelastic properties of the adhesive. Six different states of pre-loading are used. In the third section, experimental results are presented. The paper ends with conclusions and discussion.

2 Simulations

Numerical simulations are made in order to quantify the influence of a plastically or damaged zone heading the crack tip. The simulations are performed with ABAQUS v. 6.6. The cohesive properties of the adhesive are given in Fig. 2 and have been reported in earlier studies (Andersson and Biel 2006). The cohesive law for the virgin material, $\sigma_v(w)$, is extended to unloading by two hypothetical models: *elastic-plastic* (EP) and *elastic-damage* (ED), cf. Fig. 4. Note that the unloading path for the ED-model is assumed extended with the virgin elastic stiffness in the compressive range of stress. Here, w_{pd} and σ_{pd} denote the maximum deformation and corresponding stress before unloading, respectively.

Adherends are made of tool steel (Rigor Uddeholm). Tensile tests show the yield strength to be larger than 500 MPa and Young's modulus 213 GPa. The adherends are elastic during the experiments. Table 1 gives the dimensions of the specimens, for notation cf. Fig. 3. Loading the specimen results in a process zone of substantial extension compared to the height and width of the specimen (Andersson and Biel 2006). Thus, beam theory is adequate to capture the behaviour of the specimen, cf. Östlund and Nilsson (1933)).

The FE-model facilitates the symmetry of the specimen. It consists of 8800 beam- and 8001 non-linear spring-elements which represent adherends and the adhesive layer, cf. Fig. 5. The behaviour of the springs

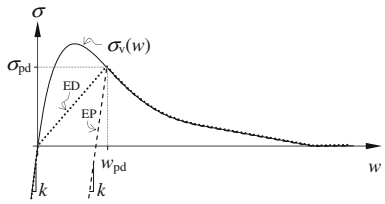

Fig. 4 Models for elastic-plastic (EP) and elastic-damage (ED) cohesive laws

Table 1 Geometry of the specimen

Unbonded length	$a = 80$ mm
Length	$l = 165$ mm
Height	$h = 6.4$ mm
Width	$b = 5.0$ mm
Layer thickness	$t = 0.2$ mm

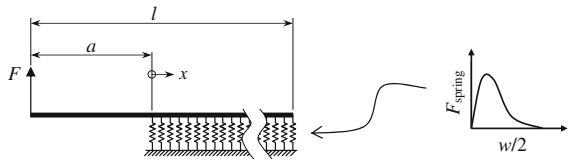

Fig. 5 The FE-simulation of the specimen with non-linear spring and beam elements

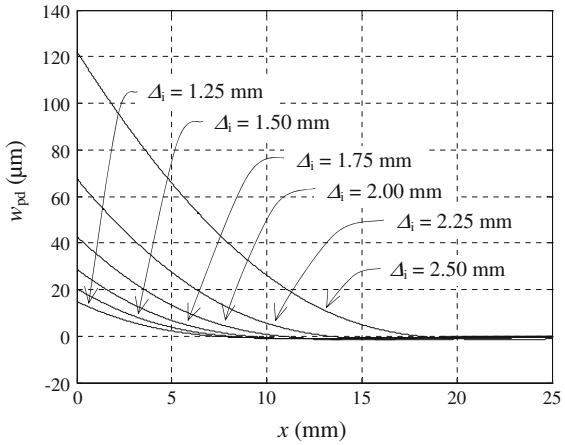

Fig. 6 The defection of the beam during the pre-loading; $x = 0$ corresponds to the start of the adhesive layer

is adapted to the cohesive properties of the adhesive layer; cf. Fig.'s 2 and 4. The force in the springs are given by,

$$F_{\text{spring}}(w/2) = A\sigma(w) \tag{5}$$

where A is the adhesive area connected to each spring, i.e. determined by the width of the specimen, b, and the distance between the springs d. For the first spring at the start of the adhesive layer, the area is $A = bd/2$. For all the other springs, the area is $A = bd$

The degradation of the adhesive layer is determined by the maximum elongation, $w_{pd}(\Delta_i, x)$ achieved during the pre-loading stage. This elongation is determined with a FE-simulation where all the springs follow the virgin cohesive law, $\sigma_v(w)$, cf. Fig. 2. The elongation, w_{pd}, is given in Fig. 6 for the six initial deflections, Δ_i, used in the experiments.

According to the deformation achieved during the pre-loading, the springs are degraded. The material behaviour used to simulate the elastic-plastic and the elastic-damage models during unloading and reloading are shown in Fig. 4. As expected, the plastic deformation of the elastic-plastic model leads to a state of

compression at the start of the adhesive layer after unloading. For this model, the degraded stress-elongation relation is given by

$$\sigma_{\mathrm{EP}} = \begin{cases} k w - k w_{\mathrm{pd}} + \sigma_{\mathrm{pd}} & w < w_{\mathrm{pd}} \\ \sigma_{\mathrm{v}}(w) & w_{\mathrm{pd}} < w < \infty \end{cases} \quad (6)$$

where $k = 10 \cdot 10^{12}$ N/m^3 is the initial stiffness corresponding to Young's modulus of 2.0 GPa for the adhesive; w_{pd} is the maximum elongation experienced during the pre-loading, σ_{pd} is the corresponding maximum stress, and $\sigma_{\mathrm{v}}(w)$ the initial, virgin, cohesive law. For the elastic-damage model, unloading leaves the adhesive layer stress free. The stress-elongation relation for the degraded elastic-damage model is given by,

$$\sigma_{\mathrm{ED}} = \begin{cases} k w & w < 0 \\ \frac{\sigma_{\mathrm{pd}}}{w_{\mathrm{pd}}} w & 0 < w < w_{\mathrm{pd}} \\ \sigma_{\mathrm{v}}(w) & w_{\mathrm{pd}} < w < \infty \end{cases} \quad (7)$$

By use of Eq.'s 6 and 7, the force-elongation relations of the springs are degraded in order to achieve the correct properties according to the pre-loading sequence and the assumed constitutive model. The F-Δ-curve and the w-Δ-curve for the reloading with $\Delta_i = 2.25$ mm are shown in Fig. 7.

As shown, the elastic-plastic model gives a permanent deformation for the adhesive layer and accordingly $F < 0$ when $\Delta = 0$ mm. When analysing the simulations of the reloading using Eq.'s 3 and 4, we assume to be ignorant of the preloading history and set the rotation, θ, and the elongation at the crack tip, w, to zero when $F = 0$. For the elastic-damage model, the zero setting is not necessary since the pre-loading does not give residual stresses or deformations. The points where the elastic-plastic curves are set to zero are indicated with dots in Fig. 7.

Figure 8 illustrates the procedure. To the left, the experimental results to be presented in the next section are shown; corresponding numerical analyses are shown in the right part. Both the pre-loading and the following reloading curves are shown. Until point A in the experimental curves, the specimen is pre-loaded; between A and B the specimen is unloaded, and after point B the reloading is performed. The dashed curves show the result without setting the values to zero after the pre-loading. For the numerical analyses, the unloading part is not necessary to simulate. Consequently, the vertical lines AB separate the pre-loading from the re-loading in the simulations. The solid curves in these graphs correspond to the elastic-damage model and the dashed curves correspond to the elastic-plastic model. It should be noted that the scale "time" is immaterial in the simulations since we assume no rate effects.

All the pre-loading states are analysed with both models, i.e. twelve simulations are performed in total. The results in Fig. 8 show that the accumulation of deformation, w, is very different between the elastic-damage and the elastic-plastic models; w increases much faster for the elastic-damage model during the re-loading stage. This results from the reduced elastic stiffness due to damage in the process region.

3 Experiments

The test equipment provides a constant loading rate of about 10 μm/s. The elongation of the adhesive layer, w is measured using two LVDTs, one on each side of the specimen. The force F is measured with a load cell and the rotation θ is measured with an incremental shaft encoder which provides $2 \cdot 10^5$ pulses per revolution. The displacement of the loading points is measured with a dial indicator; cf. Fig. 9.

In order to determine relevant values for the initial deflection of the loading point, Δ_i, of the pre-loading

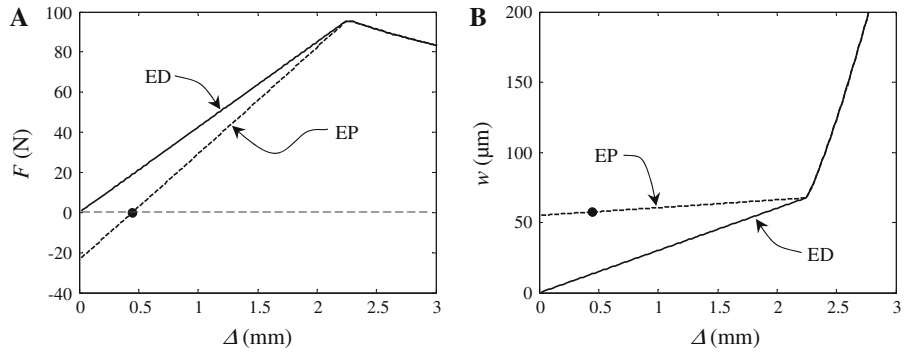

Fig. 7 Reloading **a**: Force vs. deflection and **b**: Elongation of the adhesive at the start of the layer vs. deflection of the loading point for the simulations with $\Delta_i = 2.25$ mm. Solid line elastic-damage and dashed line elastic-plastic model

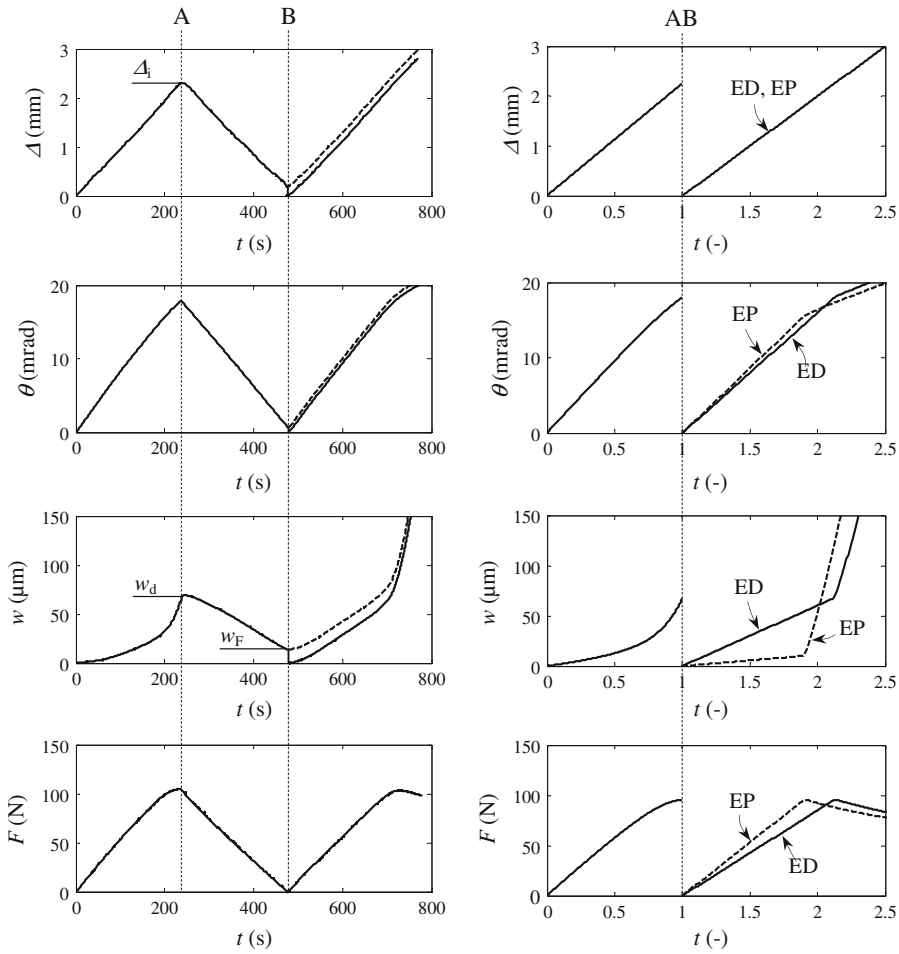

Fig. 8 Experimental- (*left*) and numerical- (*right*) results from a specimen with $\Delta_i = 2.25\,\text{mm}$

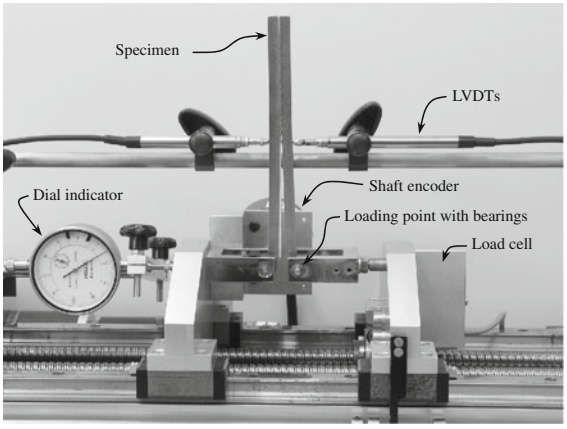

Fig. 9 Experimental setup with DCB-specimen

sequence, two experiments are performed to determine the relation between Δ and the elongation of the adhesive layer, w, cf. Fig. 10. The experiments show that the major part of the softening of the adhesive occurs for displacements of the loading points between 2.0 and 2.4 mm.

Photographs of the first 3 mm of the adhesive layer are shown in Fig. 11 at three states of loading. At, $w = 50\,\mu\text{m}$ the adhesive layer has been damaged and a noticeable stress whitening is observed. At, $w = 80\,\mu\text{m}$, micro cracks are visible and the stress is reduced to a low level, cf. Fig. 2.

Forty experiments with pre-damaged DCB-specimens are performed. Six different maximum values of the initial deflection, Δ_i between 1.25 and 2.50 mm are used. These pre-loadings correspond to $J = 40$, 50, 70, 85, slightly less than 100 and slightly larger than 100% of J_c. Four examples of the initial loading cycles are shown in Fig. 12a. During the first part of the curve, up to a load of about 20 N and a deformation of about 3 μm, the specimen behave linearly elastic. After this point,

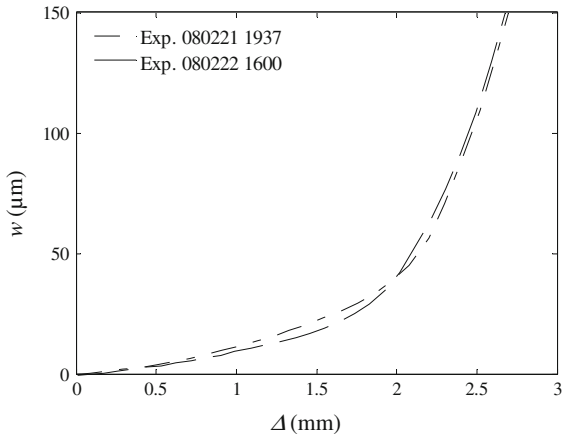

Fig. 10 The deflection of the loading points, Δvs. the elongation of the adhesive layer at the start of the layer, w for two experiments

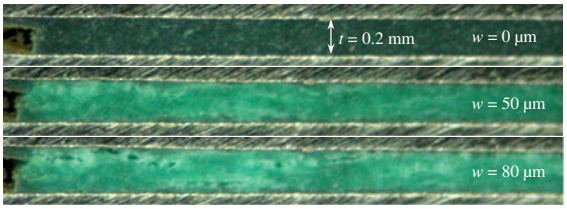

Fig. 11 Photographs taken at the start of the adhesive layer at three different stages of deformation

the adhesive yields. When Δ_i is attained, the machinery is reversed and the force begins to decrease. The smooth right ends of the curves with $\Delta_i = 2.00$ mm and $\Delta_i = 2.25$ mm indicate that the deformation process continues although unloading has begun, i.e. Δ decreases and w still increases. The unloading curves have a slight S-shape. Figure 12b shows the evolution of J according to Eq. 3. It should be noted that the measured value is not expected to be J during reloading since the adhesive is in-elastic and have properties

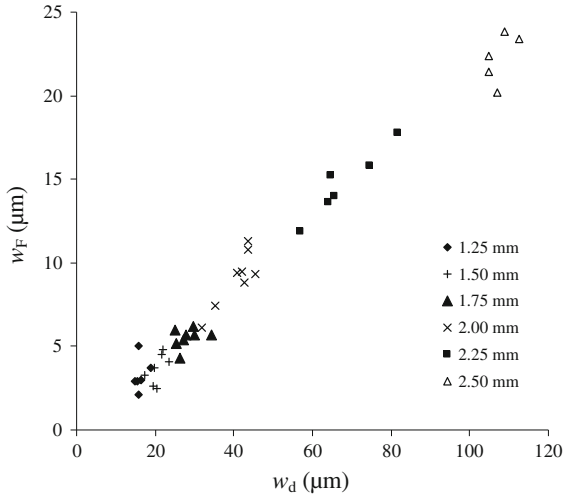

Fig. 13 Remaining deformation, w_F vs. maximum deformation, w_d after unloading in the pre-loading sequence

dependent on x, we therefore introduce the notation J^*. The J^*-w-curves show the characteristic initial parabolic shapes reflecting linear elastic behaviour of the adhesive layer at small deformations.

When the load is removed, some elongation, w_F, remains. For all experiments, this amount to about 20% of the elongation when the machinery is reversed, w_d, cf. Fig. 13.

When the force is zero in the unloading phase, all measurement devices are zeroed and the machinery is immediately reversed to start reloading of the specimen. The experimental results are presented in Fig's. 14 and 15. Figure 14 shows J^*vs. the elongation of the adhesive layer, w. The slopes of the curves are decreasing with an increase of initial damage.

Figure 15 shows the evaluated stress vs. deformation of the adhesive layer. The maximum stress, the deformation at maximum stress, and the critical deformation are all influenced by the pre-loading.

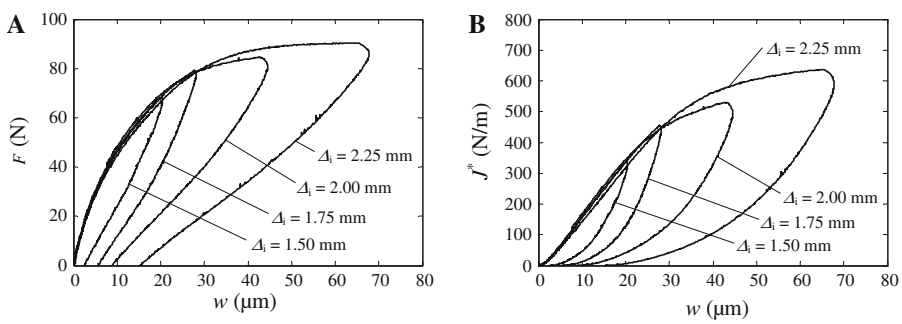

Fig. 12 Pre-load of the DCB-specimens. **a** The force vs. the elongation of the adhesive layer. **b** The virtual energy release rate vs. the elongation of the adhesive layer

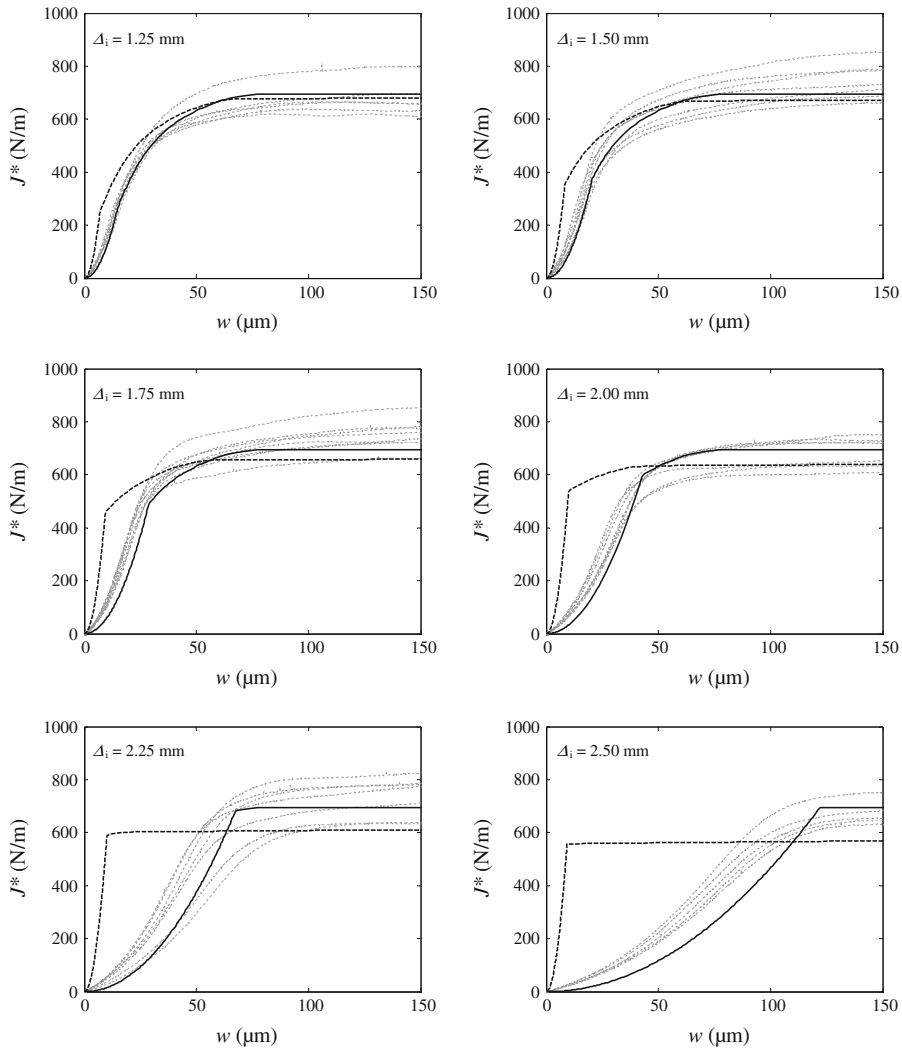

Fig. 14 J^*vs. elongation of the layer. *Solid curves* correspond to simulations with the elastic-damage model and the *dashed curve* to simulations with the elastic-plastic model. Experimental results are shown as *grey dashed lines*

Figure 16a shows the maximum stress σ_m^*vs. corresponding deformation w_m^*. Two important observations can be made; for small pre-loading, the maximum stress is increasing and for large pre-loading, non-zero cohesive stresses are evaluated although the crack has started to propagate. Figure 16b shows the apparent fracture energy, J_c^*vs. the corresponding critical deformation, w_c^*, for all forty experiments. The measured critical fracture energy J_c^* and the critical deformation w_c^* are taken when the evaluated cohesive stress is lowered to 5% of the maximum stress. The fracture energy seems almost unaffected by the initial deformation but the critical deformation increases with initial damage.

4 Comparisons experiments and simulations

Figures 14 and 15 show distinctive differences between the simulation results using the elastic-plastic and the elastic-damage model. With the elastic-plastic model, the fracture energy, corresponding to the horizontal asymptote, is somewhat smaller than the fracture energy of the virgin cohesive law used as input. This is understood from the residual deformation after the pre-loading sequence. The residual, θ, contributes to J; cf. Eq. 3. If, as assumed in the evaluation this residual θ is unknown and assumed to be zero, an apparently smaller J_c results. When comparing the J^*-w-curves of the simulations with the experiments, it is concluded that

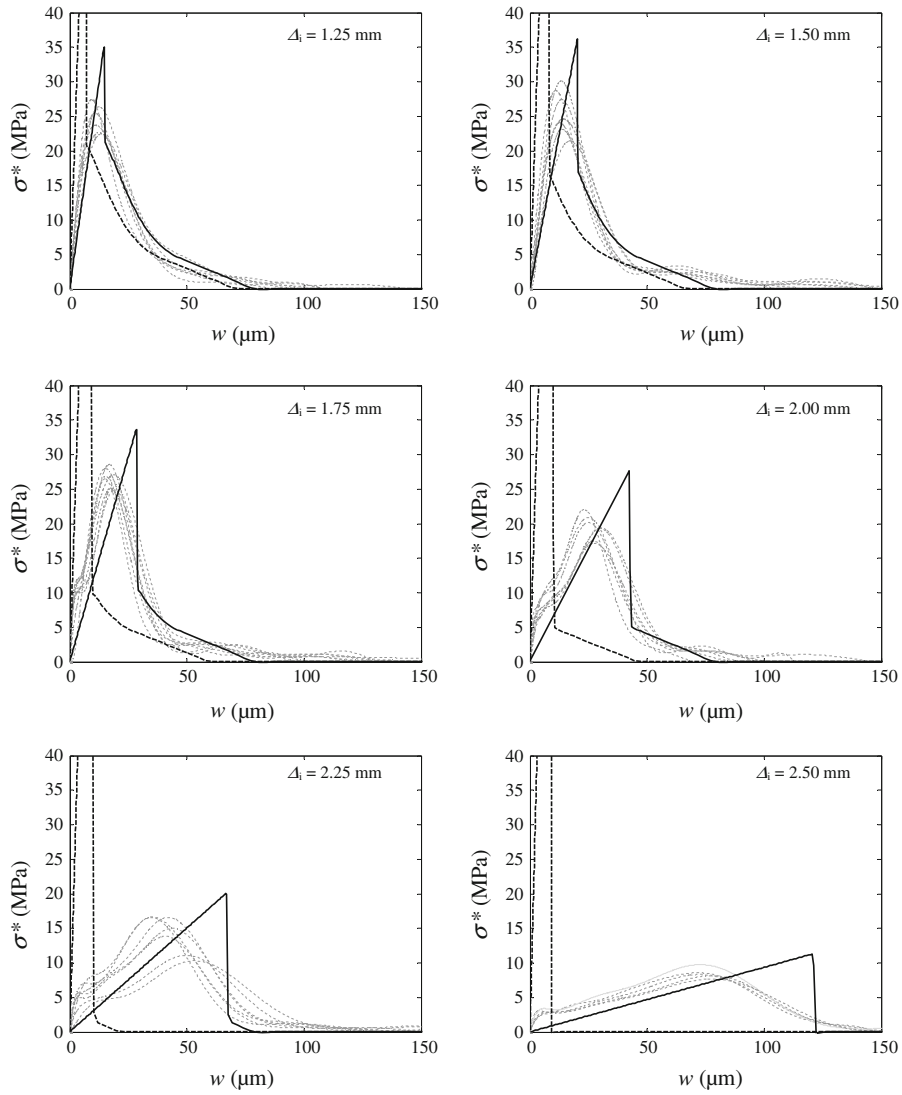

Fig. 15 Evaluated cohesive laws. *Solid curves* correspond to the elastic-damage model and the dashed curve to the elastic-plastic model. Experimental results are shown with *grey dashed lines*

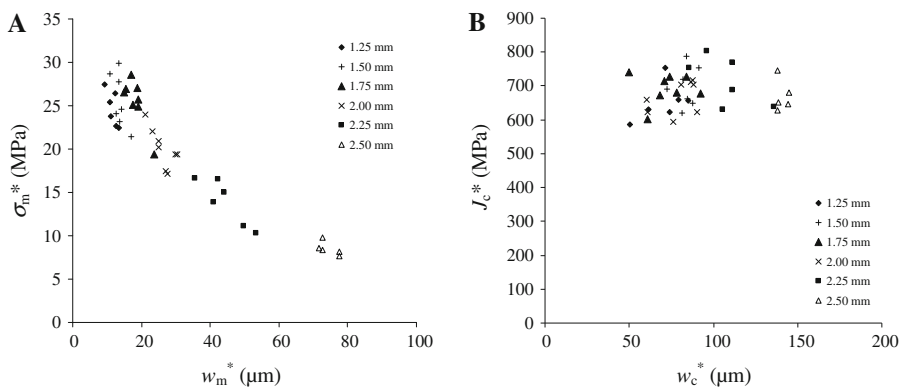

Fig. 16 Experimental results for all pre-damaged experiments with Δ_i between 1.25 and 2.50 mm. **a** Measured maximum stress vs. elongation at maximum stress and **b** Measured fracture energy vs. the critical deformation

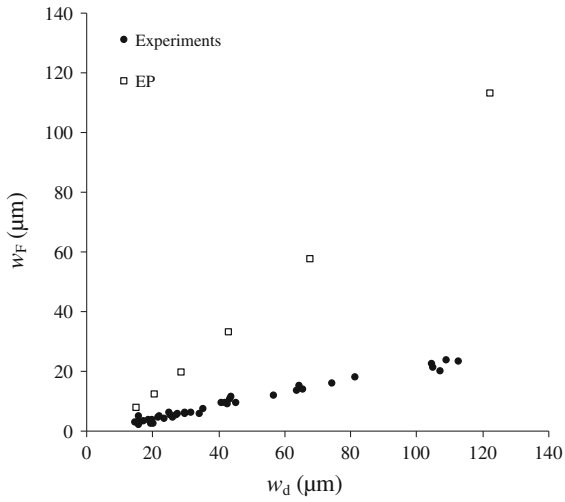

Fig. 17 Remaining deformation, w_F vs. maximum deformation, w_d after pre-loading for booth experimental and simulations with the elastic-plastic model

the cohesive law of the present adhesive is well represented by the elastic-damage model. The elastic-plastic model yields large peak stresses and less deformation at separation after pre-loading, cf. Fig. 15. As compared to the experimental results, the elastic-damage model gives good agreement. However, for all the performed experiments the remaining deformation, w_F, is about 20% of the maximum deformation, w_d, attained in the pre-loading stage. With an elastic-damage model, w_F should be zero. This indicates that some amount of plastic deformation occurs. The experimental results and the numerical simulations using the elastic-plastic model are shown in Fig. 17. As apparent, the elastic-plastic model yields a too large plastic deformation.

By introducing some amount of plasticity in the numerical simulation, the remaining deformation, w_F and evaluated energy release rate vs. deformation (J^*-w) is expected to agree better. It should be noted that the stress in the adherends is low, below about 40% of the yield strength and w_F is not believed to be due to plasticity of the adherends. A third reason for a non-zero w_F can be elastic after effects in the adhesive. That is, deformation that will disappear with time if the material is left unloaded.

The distinct cusps that appear in the simulated J^*-w-curves occur when the stressed region enters the region with non-degraded springs, cf. Fig. 14. The cusps appear both in the simulation results with the elastic-plastic and elastic-damage models. Similar features are not found in the experimental curves.

For the experiment with $\Delta_i \geq 2.00$ mm, a crack is propagating, or is about to propagate during the pre-loading sequence. In Fig. 12 it is shown that the deformation, w for these experiments increased although the machinery is reversed. This may influence the accuracy of the experiment since the size of the degraded region becomes diffuse.

The numerical analyses show that an initial degradation of the adhesive layer influences the evaluated cohesive law and that the influence is dependent on the relation between damage and plasticity. All the simulated experiments with the elastic-plastic material behaviour results in a too high maximum stress, σ_m^*. The evaluated apparent fracture energy J_c^* decreases with increasing initial degradation. With the elastic-damage material model and a small initial degradation, the maximum stress, σ_m^* increases with increasing initial degradation. With a large initial degradation, the maximum stress decreases and the critical deformation, w_c^*, increases with increasing initial degradation. With the elastic-damage material model, J_c^* is unaffected by initial degradation. In Fig. 16, most of the experiments with $\Delta_i \leq 1.75$ mm give a higher maximum stress than the virgin cohesive law; cf. Fig. 2. For the experiments with $\Delta_i \geq 2.00$ mm, most of the experiments show a decreasing maximum stress and an increasing critical deformation. Most of these results are in accordance with the elastic-damage model.

5 Conclusions

This paper presents an experimental method for deducing the relation between damage and plasticity in an adhesive layer. The method also gives some insight into effects of varying material properties along the adhesive layer. Experiments are performed using an epoxy adhesive, DOW-Betamate XW1044-3. An initial pre-load is used in order to give an initial degradation of the adhesive layer.

The experiments indicate both damage and some amount of plasticity. The method shows that damage is the major contributor to the in-elastic behaviour. In a detailed meso-mechanical analysis of the adhesive, Salomonsson and Andersson (2008) conclude that no plasticity occurs in peel loading of the present

adhesive. The validity of their simulation is improved by the result of this paper.

In experimental studies of fracture properties, pre-loading is frequently used to achieve a sharp crack tip and limit influences of an artificially machined crack. The present study indicates that the influence of these procedures might substantially influence the evaluated fracture properties, especially if the pre-loading leads to plastic deformation at the crack tip. It should be recognized that a complete cohesive law for a polymer adhesive would most likely include effects of time dependent plasticity and the Mullins effect. However, the present study shows that the main properties of a thin epoxy layer are well captured by an elastic-damage model in peel loading.

References

Alfredsson KS (2004) On the instantaneous energy release rate of the end-notch flexure adhesive joint specimen. Int J Solids Struct 41:4787–4807

Alfredsson KS, Stigh U (2004) Continuum damage mechanics revised—a principle for mechanical and thermal equivalence. Int J Solids Struct 41:4025–4045

Andersson T, Biel A (2006) On the effective constitutive properties of a thin adhesive layer loaded in peel. Int J Fract 141:227–246

Andersson T, Stigh U (2004) The stress-elongation relation for an adhesive layer loaded in modus I using equilibrium of energetic forces. Int J Solids Struct 41:413–434

Biel A (2005) Constitutive behaviour and fracture toughness of an adhesive layer. Thesis for the degree of licentiate in engineering, Chalmers University of Technology, Göteborg

Carlberger T, Stigh U (2009) Influence of layer thickness on cohesive properties of an epoxy-based adhesive—an experimental study. Accepted for publication in the Journal of Adhesion

Carlberger T, Biel A, Stigh U (2009) Influence of temperature and strain rate on cohesive properties of a structural epoxy adhesive. Int J Fract 155:155–166

Fernberg SP, Berglund LA (2001) Bridging law and toughness characterisation of CSM and SMC composites. Compos Sci Technol 61:2445–2454

Fleck NA, Hutchinson JW, Suo Z (1991) Crack path selection in brittle adhesive. Int J Solids Struct 27:1683–1703

Guo S, Dillard DA, Nairn JA (2006) The effect of residual stress on the energy release rate of wedge and DCB test specimens. Int J Adh Adhes 26:285–294

Kafkalidis MS, Thouless MD, Yang QD, Ward SM (2000) Deformation and fracture of adhesive layers constrained by plastic-deforming adherends. J Adh Sci Technol 14:1593–1607

Leffler K, Alfredsson KS, Stigh U (2007) Shear behaviour of adhesive layers. Int J Solids Struct 44:530–545

Li S, Thouless MD, Waas AM, Schroeder JA, Zavattieri PD (2006) Mixed-mode cohesive-zone models for fracture of an adhesively bonded polymer–matrix composite. Eng Fract Mech 73:64–78

Nilsson F (2001) Fracture mechanics—from theory to applications. Department of Solid Mechanics, KTH, Stockholm

Olsson P, Stigh U (1989) On the determination of the constitutive properties of the interphase layers—an exact solution. Int J Fract 41:71–76

Östlund S, Nilsson F (1993) Cohesive zone modelling of damage at the tip of cracks in slender beam structures. Fatigue Eng Mater Struct 16:663–676

Salomonsson K (2008) Mixed mode modeling of a thin adhesive layer using a meso-mechanical model. Mech Mater 40:665–672

Salomonsson K, Andersson T (2008) Modeling and parameter calibration of an adhesive layer at the meso level. Mech Mater 40:48–65

Stigh U, Andersson T (2000) An experimental method to determine the complete stress-elongation relation for a structural adhesive layer loaded in peel. In: Williams JG, Pavan A (eds) Fracture of polymers, composites and adhesives, vol 27. ESIS publication, pp 297–306

Stigh U, Alfredsson KS, Andersson T, Biel A, Carlberger T, Salomonsson K (2009) Some aspects of cohesive models and modelling with special application to strength of adhesive layers. Submitted

Sørensen BF (2002) Cohesive law and notch sensitivity of adhesive joints. Acta Materialia 50:1053–1061

Sørensen BF, Jacobsen TK (1998) Large-scale bridging in composites: *R*-curves and bridging laws. Composites part A 29:1443–1451

Suo Z, Bao G, Fan B (1992) Delamination *R*-curve phenomena due to damage. J Mech Phys Solids 40:1–16

Tvergaard V, Hutchinson JW (1996) On the toughness of ductile adhesive joints. J Mech Phys Solids 44:789–800

Zhu Y, Liechti KM, Ravi-Chandar K (2009) Direct extraction of rate-dependent traction-separation laws for polyurea/steel interfaces. Int J Solids Struct 46:31–51